PERGAMON

International Journal of Heat and Mass Transfer 45 (2002) 267–277

International Journal of HEAT and MASS TRANSFER

www.elsevier.com/locate/ijhmt

Magnetizing force modeled and numerically solved for natural convection of air in a cubic enclosure: effect of the direction of the magnetic field

Toshio Tagawa, Ryoji Shigemitsu, Hiroyuki Ozoe *

Institute of Advanced Material Study, Kyushu University, Kasuga Koen 6-1, Kasuga 816-8580, Japan

Received 6 October 2000; received in revised form 20 April 2001

Abstract

Magnetizing force is modeled by considering magnetic susceptibility as a function of temperature and is included in a momentum balance equation as an external force term in addition to the buoyant force term. Under ideal gas behavior, the magnetizing force term can be represented by a new and simple non-dimensional parameter group γ, which represents the ratio of magnetizing force to the gravitational force. This magnetizing force acts on material of high magnetic susceptibility, like oxygen gas in a temperature gradient field, and affects the convection in addition to gravity. Sample computation was carried out for air in a cubic box that is heated from one vertical wall and cooled from the opposing wall, and has the other four walls thermally insulated. With an increase in the magnetic strength, the upward and downward natural convection in the gravity field becomes horizontal circulation under a cusp-shaped magnetic field.

1. Introduction

Magnetizing force, which attracts iron filings to a permanent magnet, acts on material of high magnetic susceptibility, like iron, and not on materials like air, water and wood. However, among non-metallic materials, oxygen has a relatively high magnetic susceptibility because of its twin electronic spin; some typical values of such materials are listed in Table 1 [1]. Faraday [2] found this force works to collect oxygen gas bubbles to the center of a permanent magnet. Pauling et al. [3] employed this force to develop an oxygen analyzer. Until recently, however, this effect has been largely neglected in the field of engineering. The recent development of a superconducting magnet now allows a much stronger magnetic field to be used for various industrial purposes.

Wakayama and co-workers [4–8] have been active in finding new and notable effects of a strong magnetic field in fluid convection. The so-called Wakayama jet [8] occurs in a strong magnetic gradient field due to the difference in magnetic susceptibility between air and nitrogen gas. They also reported such phenomena as sustainable combustion in a microgravity field, the downward candle flame and enhanced flow rates of air supply. Kitazawa and co-workers [9–12] also have found various interesting phenomena such as non-mechanical blowing of heated air in a strong magnetic gradient field, enhanced oxygen gas dissolution in water, water droplet levitation and enhanced curvature of water level surface.

In the present report, the magnetizing force is modeled for convection of gas with a temperature gradient, and sample computations were carried out for natural convection of air in a cube.

2. System considered

Fig. 1 shows three cases in which a pair of electric coils is used to produce magnetic fields in the fluid in a cubic enclosure that is heated from one vertical wall and cooled from the opposing wall but otherwise thermally insulated. The geometries of the coils and the

* Corresponding author. Tel.: +81-92-583-7834; fax: +81-92-583-7838.

E-mail address: ozoe@cm.kyushu-u.ac.jp (H. Ozoe).

0017-9310/02/$ - see front matter
PII: S0017-9310(01)00149-1

Nomenclature

$\vec{B}$	$\vec{b}/b_a$ (dimensionless)
$\vec{b}$	magnetic induction (b_x, b_y, b_z) ($T = Wb/m^2 = V\ s/m^2$)
b_a	$\mu_m i/\ell$ (Wb/m^2)
$\vec{f}_m$	magnetizing force defined in Eq. (1) (N/m^3)
g	acceleration coefficient of gravity (m/s^2)
Gr	$\{g\beta(\theta_h - \theta_c)\ell^3\}/\nu^2$ (dimensionless)
$\vec{H}$	magnetic field $= \vec{b}/\mu_m$ (A/m)
i	electric current in a coil (A)
ℓ	length of a cubic enclosure (m)
P	p'/p_a (dimensionless)
p	pressure (N/m^2)
p_0	reference pressure without convection of gas (N/m^2)
p'	perturbed pressure due to convection (N/m^2)
p_a	$\rho_0(\alpha/\ell)^2$ (N/m^2)
Pr	Prandtl number $= \nu/\alpha$ (dimensionless)
R	$\lvert\vec{R}\rvert$ (dimensionless)
$\vec{R}$	$\vec{r}/\ell$ (dimensionless)
$\vec{r}$	position vector (m)
R_g	universal gas constant (J/kg K)
Ra	$Gr\ Pr$ (dimensionless)
$\vec{S}$	$\vec{s}/\ell$ (dimensionless)
$\vec{s}$	a periphery line of a coil (m)
$d\vec{s}$	tangential vector of a coil element (m)
T	$(\theta - \theta_0)/(\theta_h - \theta_c)$ (dimensionless)
t	time (s)
t_a	ℓ^2/α (s)
$\vec{U}$	$\vec{u}/u_a$ (dimensionless)
$\vec{u}$	velocity vector (u, v, w) (m/s)
u_a	α/ℓ (m/s)
X	x/ℓ (dimensionless)
x	a coordinate (m)
Y	y/ℓ (dimensionless)
y	a coordinate (m)
Z	z/ℓ (dimensionless)
z	a coordinate (m)

Greek symbols

α	thermal diffusivity of gas (m^2/s)
β	volumetric coefficient of expansion of gas due to temperature difference (1/K)
γ	$\xi\chi_{O_2}b_a^2/(g\mu_m\ell)$ (dimensionless)
θ	temperature (K)
μ	viscosity of gas (Pa s)
μ_m	magnetic permeability (H/m)
ν	kinematic viscosity of gas $= \mu/\rho_0$ (m^2/s)
ρ	density of gas (kg/m^3)
ρ_0	density of gas at a reference state of no convection (kg/m^3)
τ	t/t_a (dimensionless)
ξ	mass fraction of oxygen at some reference state (air) (dimensionless)
χ_{O_2}	magnetic susceptibility of oxygen (m^3/kg)

Subscripts

a	reference value
0	reference state
c	that of a cold plate
h	that of a hot plate

Table 1
Magnetic susceptibility (dimensionless value) for gas at 1 atm and 0°C [1]

$H_2 = -2.23 \times 10^{-9}$
$N_2 = -6.8 \times 10^{-9}$
$O_2 = 1.91 \times 10^{-6}$

enclosure are allocated as follows. The two coils are 0.1 m in diameter and are set in parallel 0.1 m apart. Centered between them is a cubic enclosure with sides of 0.064 m. The coils are located in three different orientations as shown in Figs. 1(a)–(c). The natural convection of air in an enclosure with these coils is considered herein.

3. Derivation of model equation including magnetizing force

According to Bai et al. [8], magnetizing force for air is expressed as follows:

$$\vec{f}_m = \frac{\mu_m}{2}\chi_{O_2}(\theta)\xi_{O_2}\rho\nabla H^2. \tag{1}$$

Considering $\vec{b} = \mu_m\vec{H}$ and abbreviating $\chi = \chi_{O_2}$ and $\xi = \xi_{O_2}$, this can be changed as follows in terms of magnetic induction $\vec{b}$ for air:

$$\vec{f}_m = \frac{1}{2\mu_m}\rho\chi\xi\nabla b^2. \tag{2}$$

This force can be included in the Navier–Stokes equation as an external force in addition to a buoyant force as follows:

$$\rho\frac{D\vec{u}}{Dt} = -\vec{\nabla}p + \mu\nabla^2\vec{u} + \frac{\rho\chi\xi}{2\mu_m}\vec{\nabla}b^2 + \rho\vec{g}. \tag{3}$$

This equation can be reformed as follows following the way for modeling natural convection so that numerical computation becomes much easier. The magnetizing force term is proportional to the gradient of the square of magnetic induction and can be treated similarly to pressure. Thus, when the magnetic susceptibility χ and density ρ are constant, there will be no convection. Let

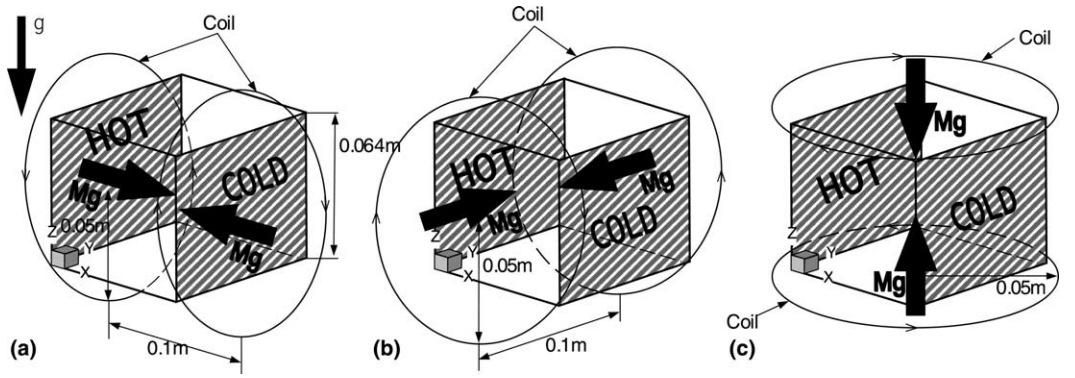

Fig. 1. Schema of the system: (a) under an X-directional magnetic field; (b) under a Y-directional magnetic field; (c) under a Z-directional magnetic field.

us assume that this state to be represented by $\theta = \theta_0$, $\rho = \rho_0$, $\chi = \chi_0$ and $p = p_0$. In this situation, velocity $\vec{u} = 0$. Then Eq. (3) gives

$$0 = -\vec{\nabla} p_0 + \frac{\rho_0 \chi_0 \xi}{2\mu_m} \vec{\nabla} b^2 + \rho_0 \vec{g}. \tag{4}$$

When there is a temperature difference, the magnetic susceptibility and density change with temperature. Pressure p is expressed by a perturbed pressure term p' in addition to the static state pressure p_0

$$p = p_0 + p'. \tag{5}$$

Subtracting Eq. (4) from Eq. (3) gives

$$\rho \frac{\mathrm{D}\vec{u}}{\mathrm{D}t} = -\vec{\nabla} p' + \mu \nabla^2 \vec{u} + \frac{(\rho\chi - \rho_0\chi_0)\xi}{2\mu_m} \vec{\nabla} b^2 + (\rho - \rho_0)\vec{g}. \tag{6}$$

Magnetic susceptibility of oxygen gas is a function of temperature θ as follows, where C is a constant [8]:

$$\chi = \frac{C}{\theta}. \tag{7}$$

When temperature difference in the fluid is not large, magnetic susceptibility may be represented as follows by a Taylor expansion:

$$\rho\chi = \rho_0\chi_0 + \left\{ \frac{\partial(\rho\chi)}{\partial\theta} \right\}_0 (\theta - \theta_0). \tag{8}$$

Presuming an ideal gas, $p = \rho R_g \theta$,

$$\frac{\partial\rho}{\partial\theta} = \frac{\partial}{\partial\theta}\left(\frac{p}{R_g\theta}\right) = -\frac{p}{R_g}\frac{1}{\theta^2} = -\frac{\rho}{\theta}. \tag{9}$$

From Eq. (7),

$$\frac{\partial\chi}{\partial\theta} = \frac{\partial}{\partial\theta}\left(\frac{C}{\theta}\right) = -\frac{C}{\theta^2} = -\frac{\chi}{\theta}. \tag{10}$$

Then,

$$\frac{\partial(\rho\chi)}{\partial\theta} = -\frac{\rho}{\theta}\chi + \rho\left(-\frac{\chi}{\theta}\right) = -\frac{2\rho\chi}{\theta} = -2\beta\rho\chi. \tag{11}$$

In this equation, the volumetric coefficient of expansion for an ideal gas $\beta \fallingdotseq 1/\theta$ was employed.Eq. (8) becomes as follows:

$$\begin{aligned}\rho\chi - \rho_0\chi_0 &= (-2\beta\chi\rho)_0(\theta - \theta_0) \\ &= -2\beta\rho_0\chi_0(\theta - \theta_0).\end{aligned} \tag{12}$$

On the other hand, the buoyancy term in Eq. (6) becomes

$$\begin{aligned}\rho - \rho_0 &= \left(\frac{\partial\rho}{\partial\theta}\right)_0 (\theta - \theta_0) = \left(-\frac{\rho}{\theta}\right)_0 (\theta - \theta_0) \\ &= -\rho_0\beta(\theta - \theta_0).\end{aligned} \tag{13}$$

Then, Eq. (6) becomes

$$\begin{aligned}\rho\frac{\mathrm{D}\vec{u}}{\mathrm{D}t} = &-\nabla p' + \mu\nabla^2\vec{u} + \frac{(-2\beta\chi_0\rho_0)}{2\mu_m}(\theta - \theta_0)\xi\nabla b^2 \\ &- \rho_0\beta(\theta - \theta_0)\vec{g}.\end{aligned} \tag{14}$$

Employing the Boussinesq approximation that density is constant other than the buoyancy term, then Eq. (14) becomes

$$\begin{aligned}\frac{\mathrm{D}\vec{u}}{\mathrm{D}t} = &-\frac{1}{\rho_0}\nabla p' + \frac{\mu}{\rho_0}\nabla^2\vec{u} - \frac{\chi_0\beta(\theta - \theta_0)}{\mu_m}\xi\nabla b^2 \\ &+ g\beta(\theta - \theta_0)\begin{pmatrix}0\\0\\1\end{pmatrix}.\end{aligned} \tag{15}$$

This is the final shape of the Navier–Stokes equation including a magnetizing force term as an external force. When there is a temperature difference in the fluid, the energy equation should be solved as well as an equation of continuity.

Magnetic induction is given by Biot–Savart's law as shown below:

Table 2
Effect of grid numbers 20^3 or 30^3 on the computed average Nusselt number

Ra	Grid	$Nu_{ave.}$
10^4	20	2.056
	30	2.055
10^5	20	4.350
	30	4.339

$$\frac{D\theta}{Dt} = \alpha\nabla^2\theta, \tag{16}$$

$$\nabla \cdot \vec{u} = 0, \tag{17}$$

$$\vec{b} = -\frac{\mu_m i}{4\pi}\int \frac{\vec{r}\times d\vec{s}}{r^3}. \tag{18}$$

These equations are non-dimensionalized by the method of Hellums and Churchill [13] as follows.

Dimensionless equations are given as follows:

$$\vec{\nabla}\cdot\vec{U} = 0, \tag{19}$$

$$D\mathrm{T}/D\tau = \nabla^2 T, \tag{20}$$

$$\frac{D\vec{U}}{D\tau} = -\vec{\nabla}P + Pr\nabla^2\vec{U} - RaPr\gamma T\,\vec{\nabla}B^2 + RaPr\begin{pmatrix}0\\0\\1\end{pmatrix}T$$
$$= -\vec{\nabla}P + Pr\nabla^2\vec{U} + RaPrT\left[-\gamma\,\vec{\nabla}B^2 + \begin{pmatrix}0\\0\\1\end{pmatrix}\right], \tag{21}$$

$$\vec{B} = -\frac{1}{4\pi}\oint\frac{\vec{R}\times d\vec{S}}{R^3}. \tag{22}$$

These constitute model equations for natural convection of an ideal gas (paramagnetic fluid) in a magnetizing force field as well as a gravity force field.

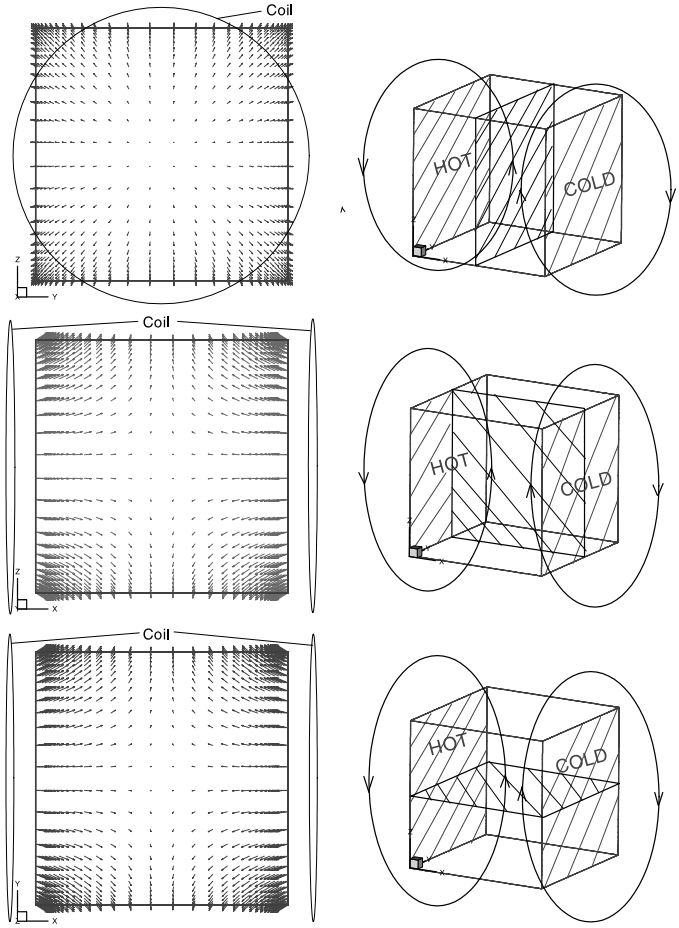

Fig. 2. Example of computed magnetic induction vectors under an *X*-directional magnetic field in a plane at $X = 0.5$, $Y = 0.5$ and $Z = 0.5$ from top to bottom.

Dimensionless variables, reference values and the characteristic dimensionless values are as follows:

$$X = x/x_a, \quad Y = y/x_a, \quad Z = z/x_a, \quad U = u/u_a,$$
$$V = v/u_a, \quad W = w/u_a, \quad P = p'/p_a,$$
$$T = (\theta - \theta_0)/(\theta_h - \theta_c), \quad B = b/b_a, \quad x_a = \ell,$$
$$u_a = \alpha/\ell, \quad b_a = \mu_m i/\ell, \quad t_a = \ell^2/\alpha, \quad p_a = \rho\alpha^2/\ell^2,$$
$$\theta_0 = (\theta_h + \theta_c)/2, \quad Pr = \nu/\alpha,$$
$$Ra = g\beta(\theta_h - \theta_c)\ell^3/(\alpha\nu), \quad \gamma = \chi_0 b_a^2 \xi/(\mu_m g \ell).$$

Here the new parameter γ represents the ratio of magnetizing force to the gravitational force. The reference value of magnetic induction b_a represents the strength of an electric current i in a coil.

The initial condition is a static state with a linear temperature profile at $\tau < 0$

$$U = V = W = 0, \quad T = 0.5 - X.$$

Boundary conditions are given as follows:

$$U = V = W = 0 \quad \text{on the wall},$$
$$T = 0.5 \quad \text{at } X = 0,$$
$$T = -0.5 \quad \text{at } X = 1,$$
$$\partial T/\partial Y = 0 \quad \text{at } Y = 0 \text{ and } 1,$$
$$\partial T/\partial Z = 0 \quad \text{at } Z = 0 \text{ and } 1.$$

Table 3
Summary of computed results for $Pr = 0.71$ and $Ra = 10^5$

	Nu (at $g = 0$ and $\gamma Ra = 10^5$)	*Nu* (at $g = 9.81$ and $\gamma = 1$)	*Nu* (at $g = 9.81$ and $\gamma = 10$)
NO-MAG	1 ($\gamma = 0$)	4.339 ($\gamma = 0$)	4.339 ($\gamma = 0$)
X-MAG	1.595	4.259	2.472
Y-MAG	2.863	4.490	6.950
Z-MAG	2.870	4.301	6.786

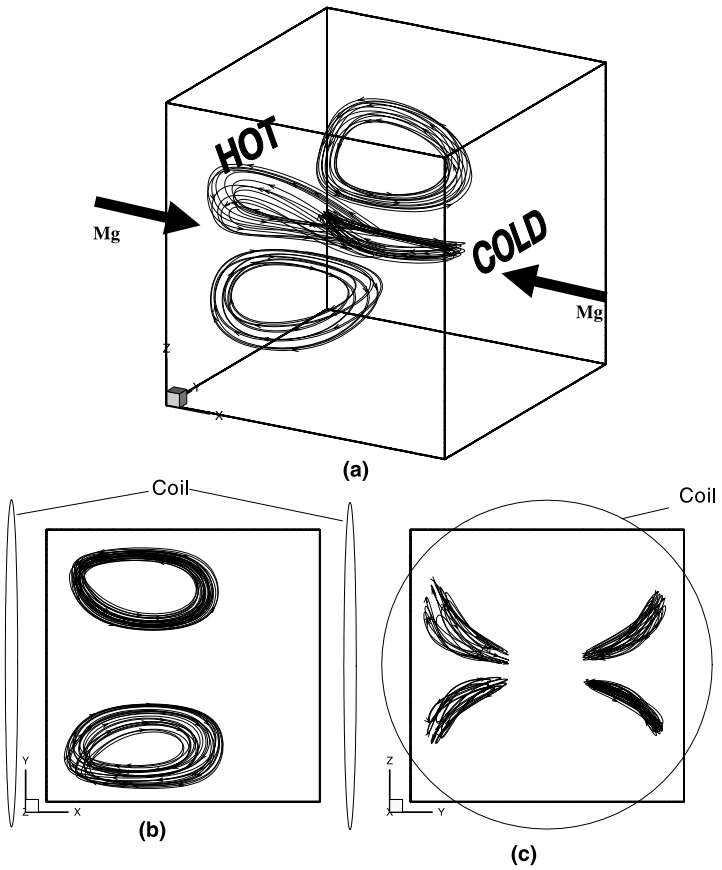

Fig. 3. Streak lines in an *X*-directional magnetic field at $\gamma Ra = 10^5$ and $Pr = 0.71$ but at $g = 0$: (a) perspective view; (b) top view; (c) end view from the positive *X*-axis.

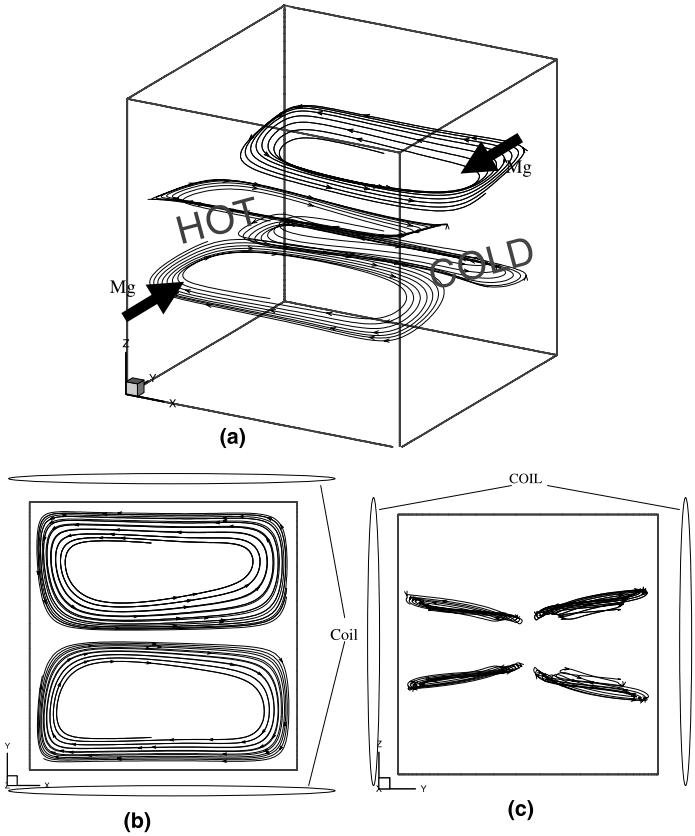

Fig. 4. Streak lines in a Y-directional magnetic field at $\gamma Ra = 10^5$ and $Pr = 0.71$ but at $g = 0$: (a) perspective view; (b) top view; (c) end view from the positive X-axis.

4. Computed results

4.1. The effect of grid size

The model equations were approximated by finite difference equations with non-uniform staggered meshes of 20^3 or 30^3. The inertial terms in the momentum equations were approximated with a third-order upwind scheme, and the HSMAC [14] method was adopted. In the range $Ra = 10^4$–10^5 for $Pr = 0.71$, the average Nusselt numbers agreed well with two grid sizes as shown in Table 2. In the present report, most of the cases studied were at $Ra = 10^5$ with grid numbers of 30^3.

4.2. Computed results in zero-gravity field

An example of a computed magnetic field is shown in Figs. 2(a)–(c) for the $X = 0.5$, $Y = 0.5$ or $Z = 0.5$ planes, respectively. Electric currents in the coils circulate in opposing directions and a cusp-shaped magnetic field is produced which has a large gradient of magnetic induction and generates a large magnetizing force.

Numerical computations were carried out first for the zero-gravity field ($g = 0$) to clarify the effect of magnetizing force field alone under a X-, Y- or Z-directional magnetic field as shown in Table 3. Even for this case of $g = 0$, $\gamma Ra = 10^5$. The average Nusselt numbers for the three different orientations of magnetic field at $\gamma = 1$ are similar for the Y- and Z-directions but different for the X-direction.

Computations were next carried out for a normal gravity field and at $\gamma = 1$. The average Nusselt numbers for various magnetic fields are similar to each other, including that at no magnetic field ($\gamma = 0$ and only gravity acts).

Further computations were carried out for a much stronger magnetic field at $\gamma = 10$. Then the average Nusselt number in the X-direction decreased and those in the Y- and Z-directions gave much larger but similar values. The magnitude of magnetic strength γ appears to have a significant effect. However, these results are quite complicated and more detailed information on velocity and temperature contours is required in order to understand these heat and flow characteristics.

The effect of the magnetizing force on the convection may be most effectively represented by streak lines based on the computed velocity fields as follows:

Figs. 3–5 show long-time streak lines for the X-, Y- or Z-directional magnetic field at $Pr = 0.71$ and $\gamma Ra = 10^5$ but $g = 0$. For the sake of explanation, we turn first to the case of the Y-directional magnetic field.

Fig. 4 shows four streak lines under the Y-directional magnetic field. Two of them can be seen from the top of the cube and are perpendicular to the usual

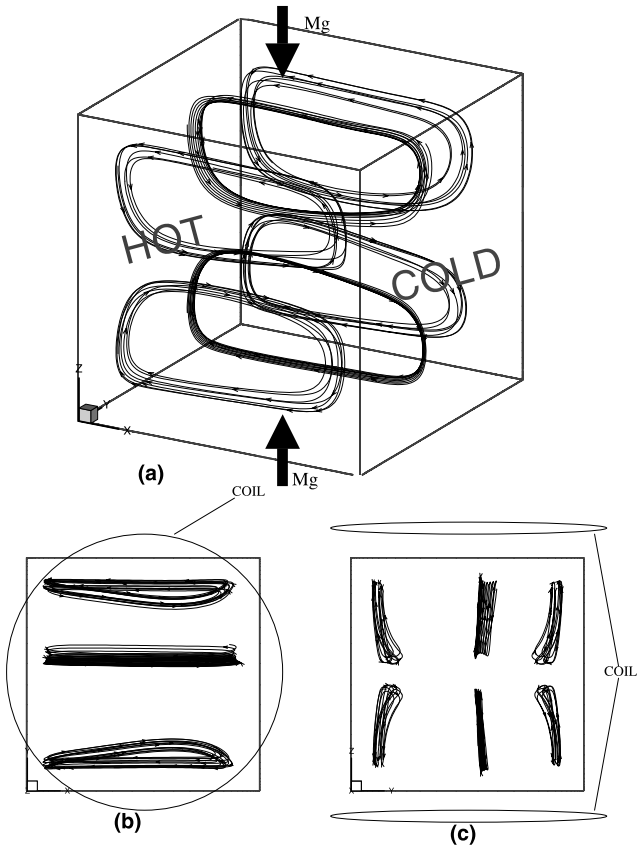

Fig. 5. Streak lines in a Z-directional magnetic field at $\gamma Ra = 10^5$ and $Pr = 0.71$ but at $g = 0$: (a) perspective view; (b) top view; (c) end view from the positive X-axis.

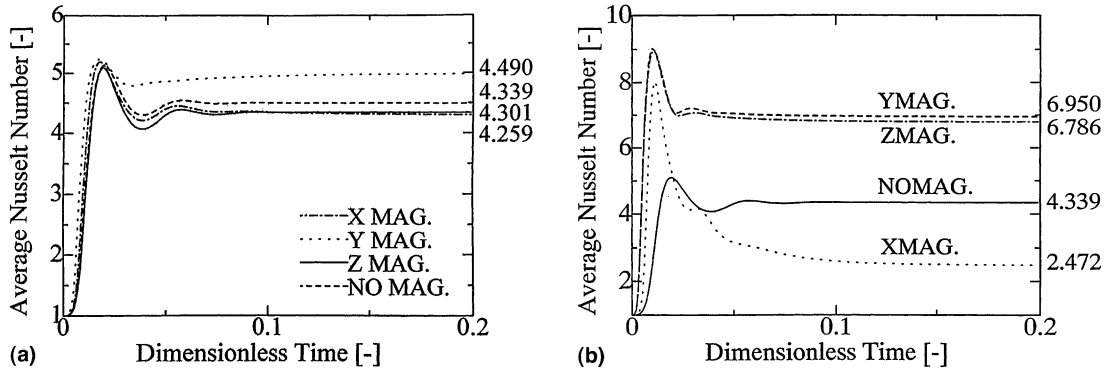

Fig. 6. Transient responses of the average Nusselt number at $Ra = 10^5$ and $Pr = 0.71$ under various magnetic fields: (a) $\gamma = 1$; (b) $\gamma = 10$.

Table 4
Dimensional equivalence under the Y-directional magnetic field for air at 300 K and 0.1 MPa

$Ra = 10^5$, $Pr = 0.71$, $\gamma = 1$, $Nu_{ave.} = 4.49$
$\ell = 0.064$ (m), $b_a = 1.558$ (T = Wb/m^2), $u_{max} = 0.37$ ($U_{max} = 10.55$) (cm/s) $\theta_h - \theta_c = 4.19$ (K), $\theta_0 = 300$ (K), $q_{ave.} = 7.71$ (W/m^2)

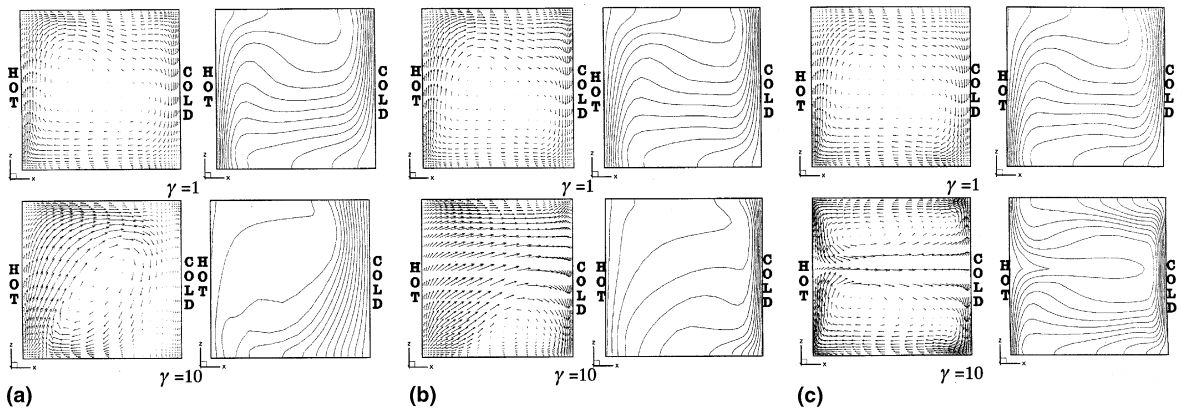

Fig. 7. Computed velocity vectors and isothermal contours at $Ra = 10^5$, $Pr = 0.71$ and $\gamma = 1$ (upper row) and 10 (lower row): (a) X-directional magnetic field; (b) Y-directional magnetic field; (c) Z-directional magnetic field.

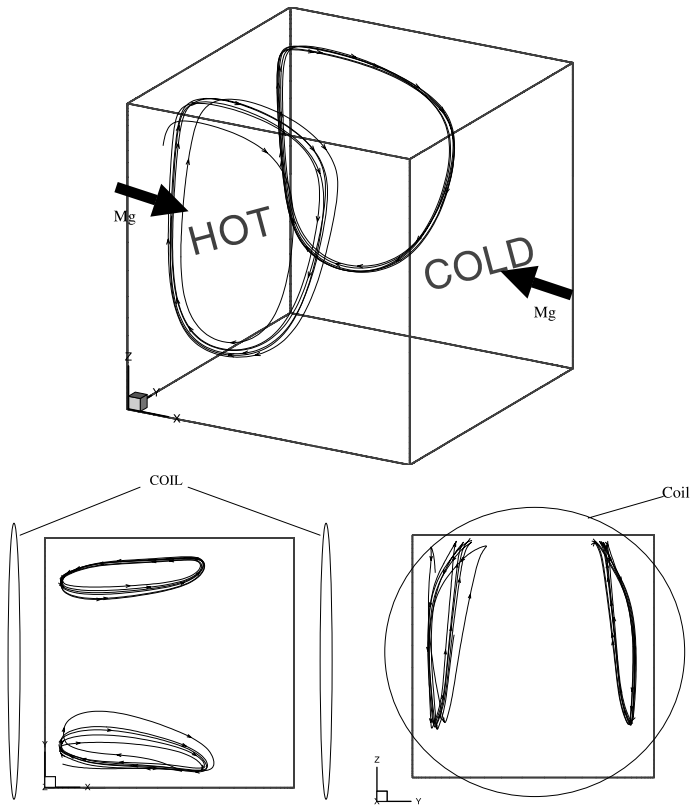

Fig. 8. Streak lines under the X-directional magnetic field at $\gamma = 10$, $Ra = 10^5$ and $Pr = 0.71$.

natural convection vortex in a gravity field. Since this is in a zero-gravity field, only the magnetizing force acts and we can see how it acts in this cusp-shaped magnetic field. Hot fluid (smaller magnetic susceptibility) is repelled from the center of the hot wall area at all levels ($Y \fallingdotseq 0.5$ and at any Z level), where the magnetic field is negligibly small. On the other hand, cold fluid (larger magnetic susceptibility) near the cold wall moves to the side walls, where the magnetic field is mostly very strong. This generates two vortices in the same level of Z, which are perpendicular to the usual vortex of natural convection in the Z-direction of a gravity field.

Fig. 5 shows six streak lines under the Z-directional magnetic field, three each in the upper and lower levels in the Z-direction. The hot fluid near the hot wall is again repelled to the core area, where the magnetic field is weak, but in this case the vortex axes are parallel to the Y-coordinate. The cold fluid near the cold wall proceeds to the top and bottom walls where the magnetic field is strong. These characteristics can be considered the same as those of the Y-directional magnetic field, since this is in a zero-gravitational field. The fluid convects in the same way in these two systems under the Y- or Z-directional magnetic field.

Let us return to the X-directional magnetic field. Fig. 3 shows four streaks under the X-directional magnetic field, which are quite different from previous two results. Under the X-directional magnetic field, the magnetic field is almost zero in the plane at $X = 0.5$. The hot fluid flows away from the hot wall area but it does not arrive at the cold wall area, since the cold fluid is attracted to the strong magnetic field there and is not repelled from the cold wall. The cold fluid is attracted to the higher magnetic field due to its larger magnetic susceptibility, the characteristics of which are included in the model derivation. Since cold fluid is stagnant near the cold wall, hot fluid cannot reach the cold wall and convects back to the hot wall.

4.3. Computed results in both gravitational and magnetizing force fields

We turn next to the system with both gravitational and magnetizing force fields.

Figs. 6(a) and (b) show transient response curves of the average Nusselt number for four cases: a gravitational field without a magnetic field, and with an X-, Y- or Z-directional magnetic field. In (a) at $\gamma = 1$, the average Nusselt numbers are similar to each other; but

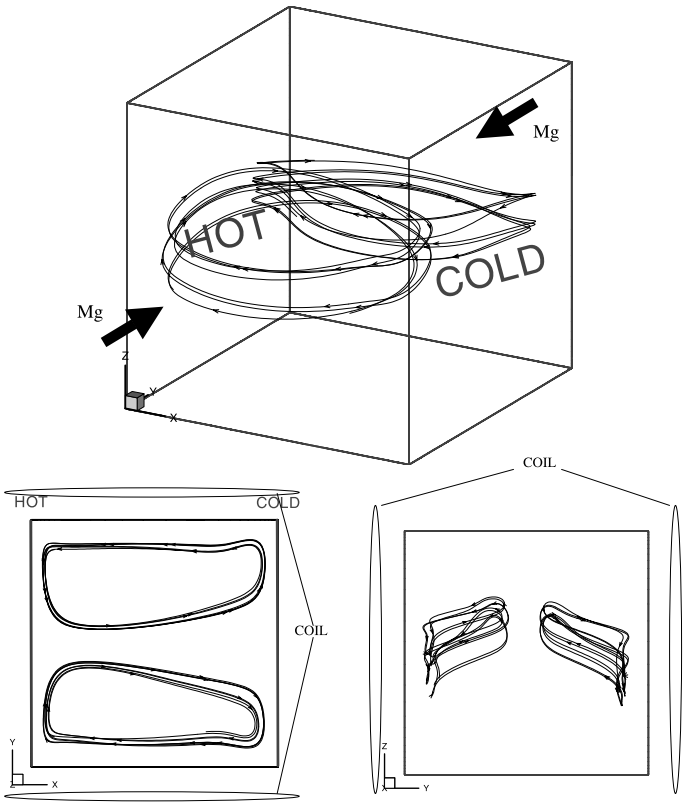

Fig. 9. Streak lines under the Y-directional magnetic field at $\gamma = 10$, $Ra = 10^5$ and $Pr = 0.71$.

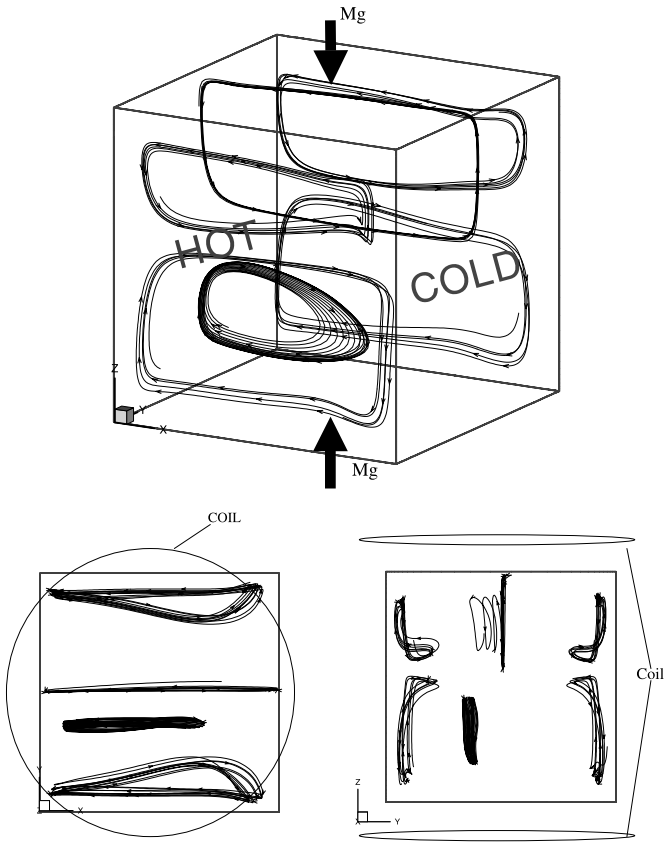

Fig. 10. Streak lines under the Z-directional magnetic field at $\gamma = 10$, $Ra = 10^5$ and $Pr = 0.71$.

in (b) at $\gamma = 10$ (4.9 T in the dimensional system), the results are quite different. With an increase in the magnetic strength, the magnetizing force appears to become dominant. The dimensional equivalence for this system is shown in Table 4.

Figs. 7(a)–(c) show velocity vectors and temperature contour maps at $\gamma = 1$ (upper row) and 10 (lower row) and at $Ra = 10^5$ and $Pr = 0.71$ for (a) X-, (b) Y- and (c) Z-directional magnetic fields under a standard gravitational field. All depict the $Y = 0.5$ vertical plane perpendicular to the hot and cold walls. For all cases of $\gamma = 1$ in (a)–(c), gravitational force is dominant and the convection mode is a familiar one in the gravitational field. However, at $\gamma = 10$, the magnetizing force becomes quite dominant and the convection modes are quite different from those at $\gamma = 1$.

Figs. 8–10 show streak lines for the system under both a gravitational and an (a) X-, (b) Y-, or (c) Z-directional magnetic field at $\gamma = 10$. Despite the presence of the gravitational field, the magnetizing force appears to be dominant, especially for Y- (Fig. 9) and Z-directional (Fig. 10) magnetic fields, where two major vortices appear with their axes in the Z-direction (Fig. 9) or the Y-direction (Fig. 10). The differences in the vortex shape from those of Figs. 3–5 are due to the combined effects of gravitational and magnetizing forces. Under the X-directional magnetic field, the convection rolls may be considered to be similar to those under a gravitational field, but the vortices do not reach the cold wall, for the reasons discussed in Fig. 3. In this sense, these vortices are also quite different from the gravitational ones. Because of this convection mode, the average Nusselt number is much smaller ($Nu = 2.47$) than in the zero-magnetic field ($Nu = 4.34$), as seen in Table 3. On the other hand, due to the direct convection from the hot wall to the cold wall as seen in Figs. 9 and 10 for the Y- or Z-directional magnetic field, the average Nusselt number takes values of 6.95 and 6.79, which are much larger than 4.34 without a magnetic field.

An experimental approach should be taken to inspect these characteristics quantitatively. However, differences in the average heat transfer rates can be observed only with a magnetic field as strong as 5 T.

5. Conclusion

Simple model equations for a non-isothermal system under a magnetizing force were derived by following the model of the Wakayama group, and the effects of gravity and the direction of magnetic field were studied numerically for air in a cubic enclosure that was heated from one wall and cooled from the opposing wall and for a cusp-shaped magnetic field applied in the X-, Y- or Z-direction. The convection of fluid can be well explained by the repulsion of hot fluid from the hot wall to the weak magnetic field and the attraction of cold fluid to the strong magnetic field; and these features are reflected in the mathematical model for a magnetizing force.

References

[1] M. Kato, Denjikigaku, Tokyo University Press, 1987 (in Japanese).
[2] M. Faraday, Philos. Mag. Soc. 3 (210) (1847) 401.
[3] L. Pauling, R.E. Wood, J.H. Sturdivant, An instrument for determining of partial pressure of oxygen in a gas, J. Am. Chem. Soc 68 (1946) 795.
[4] N.I. Wakayama, Behavior of flow under gradient magnetic fields, J. Appl. Phys. 69 (4) (1991) 2734–3736.
[5] N.I. Wakayama, Effect of a decreasing magnetic field on the flow of nitrogen gas, Chem. Phys. Lett. 185 (5–6) (1991) 449–451.
[6] N.I. Wakayama, Magnetic promotion of combustion in diffusion flames, Combust. Flame 93 (3) (1993) 207–214.
[7] N.I. Wakayama, H. Ito, Y. Kuroda, O. Fujita, K. Ito, Magnetic support of combustion in diffusion flames under microgravity, Combust. Flame 107 (1–2) (1996) 187–192.
[8] B. Bai, A. Yabe, J. Qi, N.I. Wakayama, Quantitative analysis of air convection caused by magnetic-fluid coupling, AIAA J. 37 (12) (1999) 1538–1543.
[9] Y. Ikezoe, N. Hirota, J. Nakagawa, K. Kitazawa, Making water levitate, Nature 393 (1998) 749–750.
[10] Y. Ikezoe, N. Hirota, T. Sakihama, K. Mogi, H. Uetake, T. Homma, J. Nakagawa, H. Sugawara, K. Kitazawa, Acceleration effect on the rate of dissolution of oxygen in a magnetic field, J. Jpn. Inst. Appl. Magn. 22 (4-2) (1998) 821–824 (in Japanese).
[11] H. Uetake, J. Nakagawa, N. Hirota, K. Kitazawa, Nonmechanical magnetothermal wind blower by a superconducting magnet, J. Appl. Phys. 85 (8) (1999) 5735–5737.
[12] J. Nakagawa, N. Hirota, K. Kitazawa, M. Shoda, Magnetic field enhancement of water vaporization, J. Appl. Phys. 86 (5) (1999) 2923–2925.
[13] J.D. Hellums, S.W. Churchill, Simplification of the mathematical description of boundary and initial value problem, AIChE J. 10 (1964) 110–114.
[14] C.W. Hirt, B.D. Nichols, N.C. Pomero, Los Alamos Scientific Laboratory, LA-5852, 1975.